DOI:10.1190/segam2019-3216797.1

3D Seismic Facies Classification using Convolutional Neural Network and Semi-supervised Generative Adversarial Network

Mingliang Liu[1], Weichang Li[1], Michael Jervis[2] and Philippe Nivlet[2]
1 - Aramco Research Center – Aramco Services Company, Houston, USA
2 - EXPEC ARC, Saudi Aramco

Summary

Seismic facies analysis interprets depositional environment and facies types from the reflection seismic data, an important step in exploration and reservoir characterization. While machine learning methods, especially deep learning models such as convolutional neural networks (CNNs) have been applied to assist interpretation such as salt identification, significant challenges still remain for 3D multi-class seismic facies classification: complex data representation, limited labeled data for training, imbalanced facies class distribution and lack of rigorous performance evaluation mechanism in realistic settings. In this study, we investigate the feasibility of using a supervised CNN and a semi-supervised generative adversarial network (GAN) for 3D facies classification from seismic data and well logs, to overcome these challenges. We assess the performance with varying data representations and in situations with sufficient and limited well data respectively. Unlike previous studies, the 3D facies models in this work were generated from the structural information of an onshore field and calibrated on actual well log data and core analysis and therefore, both our analysis and results provide a realistic and meaningful implication for quantitative seismic interpretation.

Introduction

Seismic facies interpretation is a fundamental and important step in exploration, reservoir characterization and field development. However, with data size of typical 3D seismic volumes drastically increasing, it becomes labor-intensive and often infeasible with manual interpretation. Over the last decades, great efforts have been made in automatic seismic interpretation to free people from the tedious manual analysis, such as seismic waveform classification using principle component analysis and artificial neural network, and seismic multi-attribute analysis with Self Organizing Map (Zhao et al., 2015). Those methods are usually unsupervised, and as a result, the results are not necessarily geologically meaningful and further interpretation is required. More importantly, their performance might heavily rely on the input features that are generally extracted empirically rather than optimally. Recently, machine learning methods, especially deep learning models such as convolutional neural networks (CNNs), have achieved promising results in seismic interpretation, i.e. fault picking (Xiong et al, 2018), multiclass structure element classification (Li, 2018), salt detection (Di et al, 2018) and seismic facies classification (Dramsch and Lüthje, 2018; Zhao, 2018). The main advantage of deep learning over the unsupervised methods mentioned earlier is its powerful ability of feature learning and hierarchical representation from large sample data sets in high dimensional space, and the ability to deal with nonlinear complexity. Each CNN convolutional layer consists of a number of filters aiming to learn different features. By stacking multiple convolutional layers together and optimizing the weight coefficients to minimize the classification loss, a CNN model is able to capture the salient feature representation most sensitive for classification.

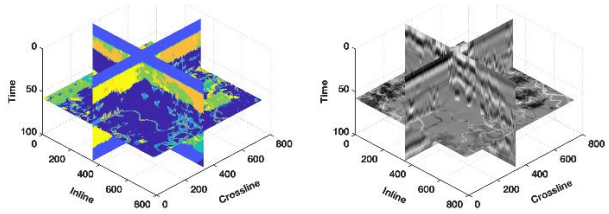

Figure 1: Synthetic lithofacies model (left) and the corresponding 3D seismic volume (right).

Although deep learning has become increasingly popular in geophysics, significant challenges remain for 3D facies classification, including data representation associated network complexity, limited labeled data for training, imbalanced facies class distribution and lack of rigorous performance evaluation in realistic settings. Previous studies in facies classification have mainly relied on manually interpreting a subset of seismic data to obtain training samples instead of calibrating against well log data. In addition, facies class distribution in the training set is not necessarily consistent with realistic settings.

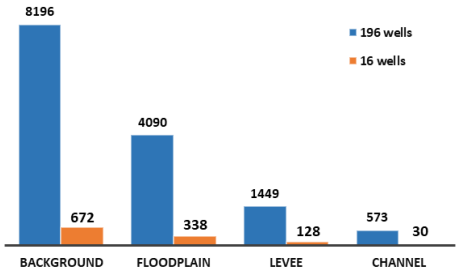

Figure 2: Histogram of facies classes in training samples with 196 (older fields) and 16 wells (new prospects), respectively. The four background facies are merged.

10.1190/segam2019-3216797.1

To address the above challenges, we use a realistic 3D facies model (Figure 1) and utilize only the information at well locations (lithofacies determined by well logs and core analysis) as labels to perform facies classification from seismic reflection data with deep neural networks. Since the amount of well data can vary from relatively abundant in older fields to extremely rare in new prospects, we propose two types of deep learning frameworks: I. Conventional CNNs relying on having a lot of labeled data; and II. A state-of-the-art semi-supervised generative adversarial network (GAN) requiring only limited well data to be incorporated in the network training process and still obtain a good result. Both approaches use convolutional layers that take various representations of 3D seismic sample data as input instead of the conventional trace-by-trace classification. As a result, the predicted facies models are more consistent with both the well and the seismic reflection data.

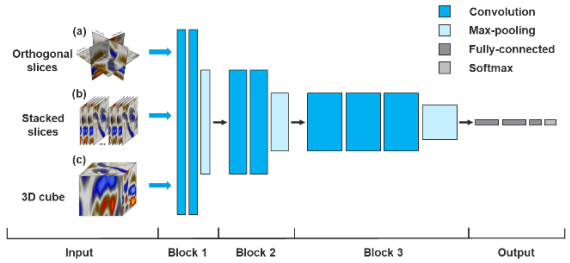

Figure 3: Architecture of the three CNN models with (a) three orthogonal seismic slices, (b) stacked time slices; (c) 3D cube as input, respectively.

Facies Model and Dataset

The data set used in this study was generated from a realistic synthetic model that mimics an existing on-shore field. The 3D facies model was built by geostatistics using lithofacies from actual wells and the structural framework from a carbonate reservoir model covering a horizontal area of approximately 620 km^2. As illustrated in Figure 1, the reservoir model consists of three units (top, middle and bottom), and in the central unit some channel and levee systems are placed in the floodplain background. There are 7 different lithofacies in total. The corresponding 3D post-stack seismic data were then generated from the P-wave velocity and density information via convolving the seismic forward model output with a 25 Hz Ricker wavelet.

In generating the model data sets, we took into account two common scenarios: older fields with relatively abundant number of wells and new prospects with very few wells. Accordingly, we selected 196 (14×14) and 16 (4×4) traces as pseudo-wells for each case respectively. We then extracted labeled samples along these pseudo-wells to form the training data set. The facies class distributions in the training sets are shown in Figure 2 for both cases.

Supervised CNN Models

As shown in the histogram in Figure 2, there are thousands of training samples with labeled facies in the case with abundant wells (channel facies have only 573 samples), which is generally sufficient to avoid the overfitting of supervised deep neural networks. For this reason, we adopt the standard CNN model as the classifier. To address computational complexity, we tried three different input representations of the seismic sample cubes and evaluated the performance of the associated CNN models including:

I. 2D CNN using three orthogonal seismic slices along inline, crossline and time axis of the sample as input;
II. 2D CNN with 2D stack of all seismic time slices of the sample cube as different channels;
III. Full 3D CNN with the entire seismic cube as input.

All three CNN models above have a similar architecture adapted from VGGNet (Simonyan and Zisserman, 2014), as illustrated in Figure 3. The differences are in the shapes of input data and the operations of convolution and pooling in 2D or 3D. In this study, we use the same sampling window size of 32×32×32 to extract training samples in all three models, with respective representations specified above.

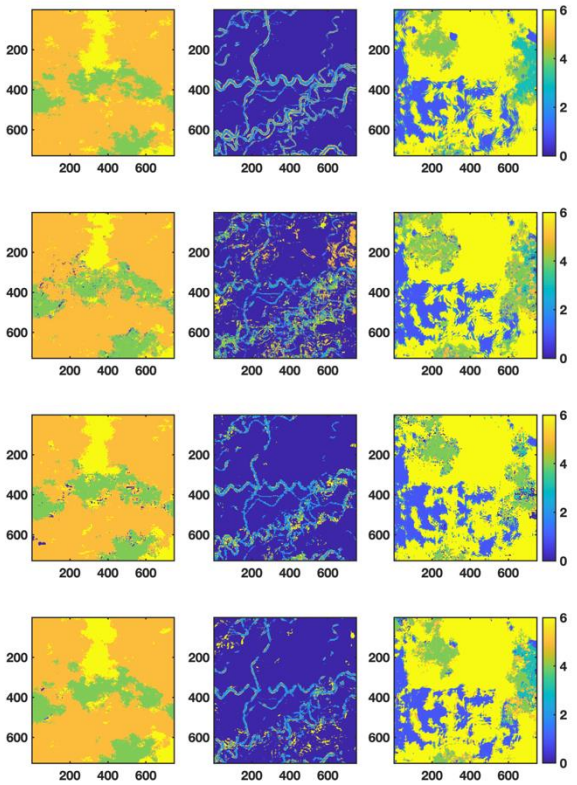

Figure 4: True lithofacies model (first row) and predicted models from orthogonal slice-based 2D CNN (second row), cube-based 2D stack CNN (third row) and cube-based 3D CNN (fourth row).

Predicted facies from all three CNNs are shown in Figure 4 for several example time slices, along with the ground truth. The prediction from the 2D CNN model using only three orthogonal slices appears significantly noisier, potentially due to the loss of certain 3D spatial information in the facies structures, especially for the channels. This noise is much lower with the other two CNN models. For a fair comparison, we adopted similar network configurations for both cube-based 2D stack CNN and cube-based 3D CNN, and overall they performed similarly. This may be attributed to the fact that the correlation length of the data in the time direction is short and therefore spatial information loss in the 2D stack representation is not that significant. The fully 3D CNN does provide better performance on certain classes (e.g. green colored class). It is also worth noting that the 3D CNN is generally more flexible in exploiting 3D spatial patterns, hence provides better class discrimination. During the tests we have found that the performance can be sensitive to the pooling size in time direction. This could be an indication that the 3D CNN performance may be further improved with optimized hyper-parameter choices.

One powerful aspect of deep learning is the ability to map the input into a learned feature space where samples belonging to different classes can be better separated. This effect can be observed in Figure 5 where the t-SNE (van der Maaten and Hinton, 2008) visualization of the original seismic data and the final layer features extracted from the cube-based 2D stack CNN are plotted. As shown, it is evident that the samples of different lithofacies, initially overlapping in the seismic data space, become separable groups in the feature space generated in the CNN model.

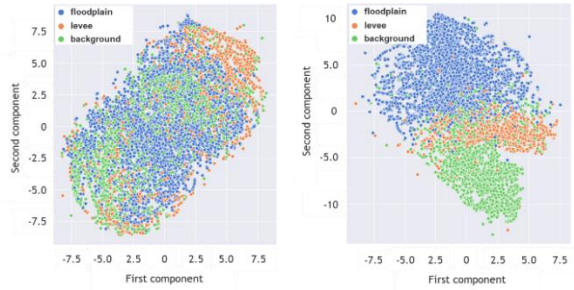

Figure 5: t-SNE visualization of original seismic data (left) and extracted features of the cube-based 2D stack CNN (right). CNN results show improved class discrimination.

Semi-supervised GAN

Although CNN models perform well when there are sufficient number of wells, hence training data samples, they fail quickly in the areas with limited well control where the number of training data samples drops and the model becomes overfitted. This greatly limits their application in practice, especially in new fields with few wells. For example, with 16 pseudo-wells in the facies model, only about 1,000 training samples with labels are available for training as shown in Figure 2. In addition, due to class imbalance, some of the under-represented facies such as channel only get very few number of samples for training (e.g. channel facies = 30 samples).

To overcome this issue, we have developed a semi-supervised method based on generative adversarial network (GAN) (Salimans et al., 2016). GAN provides a mechanism to leverage both the limited amount of labeled data and the abundant number of unlabeled data to gain more insight into the sample data space structure. Combined with CNN models, it retains the powerful ability of feature learning and representation, and if trained properly, can significantly improve classification performance in cases with training sample deficiency.

GANs consist of two competing players (Generator and Discriminator) involved in a minimax game. In classification problems, the discriminator becomes a multi-class ($\boldsymbol{K+1}$) classifier where the first $\boldsymbol{K}$ dimensions represent the classes to be classified and the last dimension indicates real or fake. In our example there are 7 original lithofacies to be classified. We convert the discriminator into an 8-class classifier: the first 7 are for the individual class probabilities of facies and the last as indicator for all the fake inputs from the generator, as illustrated in Figure 6.

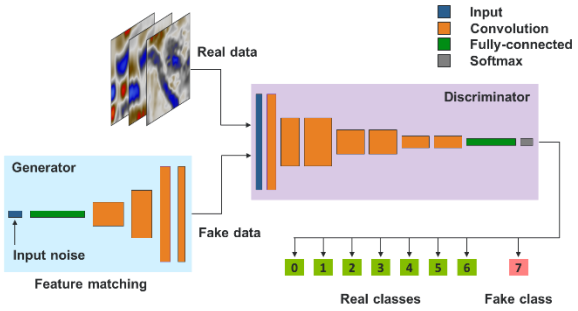

Figure 6: Architecture of the semi-supervised GAN used in this study (with max-pooling layers omitted for clarity).

The overall loss function in the discriminator has three terms associated with (1) real samples with labels, (2) real samples without labels, and (3) fake samples from the generator, as described in Equation 1.

$$\boldsymbol{L_D = L_s + L_{us}} \qquad (1)$$

where $\boldsymbol{L_s}$ and $\boldsymbol{L_{us}}$, denoting the supervised and unsupervised loss functions respectively, are given as

$$\boldsymbol{L_s = -E_{x,y\sim p_{data}(x,y)}[\log p_{model}(y|x, y < K+1)]}$$

DOI:10.1190/segam2019-3216797.1

$$L_{us} = -\{E_{x\sim p_{data}(x)}\log[1 - p_{model}(y = K+1|x)] + E_{x\sim G}[\log p_{model}(y = K+1|x)]\}$$

Feature matching is used for the generator loss so that the difference between the features of the real samples and those of the fake samples from generator are minimized instead of the difference between pixels.

$$L_G = \left\| E_{x\sim p_{data}(x)} f(x) - E_{z\sim p_z(z)} f(G(z)) \right\|_2^2 \quad (2)$$

where $f(\cdot)$ is the feature vector extracted in an intermediate layer by the discriminator.

We first trained the Generator and the Discriminator on both labeled samples extracted along pseudo-wells and unlabeled samples evenly extracted along inline, crossline and time direction. In the inference phase, the generator was discarded, and the discriminator was used for the final classification. Figure 7 shows the loss and accuracy curves of the discriminator during training and validation. We chose the ideal point to stop training around 20 epochs to minimize the possibility of overfitting.

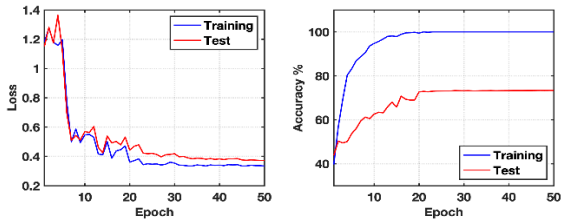

Figure 7: Discriminator loss (left) and accuracy (right) curves for training (blue) and validation (red).

The normalized confusion matrices for both the semi-supervised GAN and the CNN model evaluated on the entire volume are provided in Figure 8. We can observe that the CNN tends to misclassify channel and levee into background and floodplain facies, which are both dominant facies in this case, an indication of an overtrained network. The false-negative channel/levee predictions are from over-represented facies classes. In comparison, the semi-supervised GAN has significantly more true positives (diagonal values). While both networks have difficulty in discriminating channel from levee, potentially due to the limited resolution of the seismic data and insufficient number of total samples (labeled or unlabeled) of both facies to adequately learn their features, the GAN combined prediction totals much more than those of the CNN (65 vs 37%). Figure 9 compares predictions from the networks versus the true facies. As shown in the 3D views, the semi-supervised GAN recovers most facies with extremely limited well data, whereas the CNN performs very poorly. A zoom in on the central unit containing the channel facies, as shown on the right column, shows that most channels are predicted with a satisfactory accuracy by the semi-supervised GAN while the CNN severely misclassifies them.

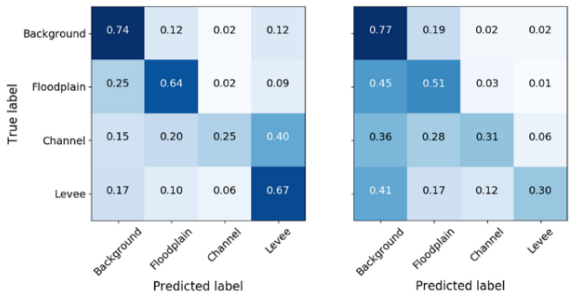

Figure 8: Confusion matrices computed for predictions from both (left) the GAN and (right) the CNN.

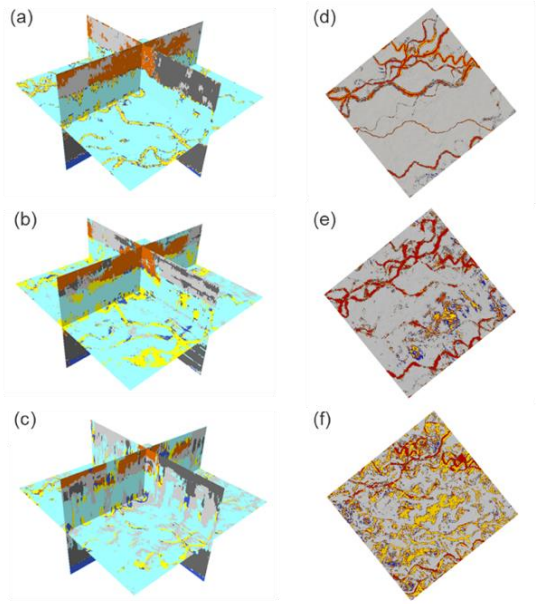

Figure 9: 3D lithofacies model showing a) ground truth, (b) GAN prediction, (c) CNN prediction and a time slice showing (d) ground truth, (e) GAN prediction, and (f) CNN prediction.

Conclusions

In this study, we propose two deep learning frameworks for 3D seismic facies classification calibrated from well log data: a fully supervised CNN for mature fields with relatively abundant well data and a semi-supervised GAN for new prospects with limited number of wells. The networks were successfully tested on realistic synthetic cases. The results show significant potential of these deep learning methods in conventional quantitative seismic interpretation workflows. They provide a robust way to combine well data and 3D seismic data to estimate lithofacies types away from areas of well control for an improved reservoir model description.

REFERENCES

Di, H., Z., Wang, and G., AlRegib, 2018, Deep Convolutional Neural Networks and seismic salt-body delineation: AAPG Annual Convention and Exhibition.

Dramsch, J. S., and M., Lüthje, 2018, Deep-learning seismic facies on state-of-the-art CNN architectures: 88th Annual International Meeting, SEG, Expanded Abstracts, doi: https://doi.org/10.1190/segam2018-2996783.1.

Li, W., 2018, Classifying geological structure elements from seismic images using deep learning: 88th Annual International Meeting, SEG, Expand Abstracts, 4643–4648, doi: https://doi.org/10.1190/segam2018-2998036.1.

Salimans, T., I., Goodfellow, W., Zaremba, V., Cheung, A., Radford, and X., Chen, 2016, Improved techniques for training GANs: Advances in Neural Information Processing Systems, 2234–2242.

Simonyan, K., and A., Zisserman, 2014, Very Deep Convolutional Networks for Large-Scale Image Recognition: Computer Visions and Pattern Recognition, arXiv: 1409.1556.

van der Maaten, L. J. P., and G. E., Hinton, 2008, Visualizing data using t-SNE: Journal of Machine Learning Research, **9**, 2579–2605.

Xiong, W., Y., Ma, Y., Wang, N. M., AlBinHassan, M. N., Ali, and Y., Luo, 2018, Seismic fault detection with convolutional neural network: Geophysics, **83**, no. 5, O97–O103, doi: https://doi.org/10.1190/geo2017-0666.1.

Zhao, T., 2018, Seismic facies classification using different deep convolutional neural networks: 88th Annual International Meeting, SEG, Expanded Abstracts, 2046–2050, doi: https://doi.org/10.1190/segam2018-2997085.1.

Zhao, T., V., Jayaram, A., Roy, and K. J., Marfurt, 2015, A comparison of classification techniques for seismic facies recognition: Interpretation, **3**, no. 4, SAE29–SAE58, doi: https://doi.org/10.1190/INT-2015-0044.1.

DOI:10.1190/segam2019-3216797.1